Journal of Materials Chemistry B

ROYAL SOCIETY OF CHEMISTRY

PAPER

Cite this: *J. Mater. Chem. B*, 2023, **11**, 7696

Quaternized carbon dots with enhanced antimicrobial ability towards Gram-negative bacteria for the treatment of acute peritonitis caused by *E. coli*†

Xintian Zhang,‡[a] Pingping Wu,‡[a] Xiaoli Hao,[a] Jiamiao Liu,[a] Zhengjun Huang,[a] Shaohuang Weng,*[a] Weifeng Chen,[b] Lingling Huang*[c] and Jianyong Huang*[b]

Received 20th April 2023,
Accepted 5th July 2023

DOI: 10.1039/d3tb00889d

rsc.li/materials-b

Infections caused by Gram-negative bacteria still pose a clinical challenge. Although nanomaterials have been developed for antibacterial treatments, a systematic evaluation of the mechanisms and intervention models of antibacterial materials toward Gram-negative bacteria is still lacking. Herein, antibacterial quaternized carbon dots (QCDs) were synthesized *via* a one-step melting method using anhydrous citric acid and diallyl dimethyl ammonium chloride (DDA). The QCDs exhibited effective broad-spectrum antibacterial activity and enhanced inhibitory ability towards Gram-negative bacteria. The antibacterial mechanism of the QCDs with respect to Gram-negative bacteria was investigated through the characterization of bacterial morphology changes, the absorption modes of the QCDs on bacteria, and the potential generation of reactive oxygen species by the QCDs. The QCDs showed low toxicity in different cells, and did not cause hemolysis. The QCDs were administered *via* intraperitoneal injection to treat acute peritonitis in mice infected with *E. coli*. Routine blood examination, magnetic resonance imaging, and pathological analysis were undertaken and it was found that, similar to the positive control group treated with gentamicin sulfate, the QCDs exhibited a therapeutic effect that eliminated infection and inflammation. This study explores a controllable synthetic strategy for the synthesis of active carbon dots with antibacterial activity, a material that is a promising candidate for new treatments of Gram-negative bacterial infections.

1. Introduction

Since the discovery of antibiotics, bacterial infections have been effectively treated. However, in recent years, the overuse and abuse of antibiotics, environmental pollution, and the transmission of drug-resistant plasmids have led to the emergence and rapid spread of drug-resistant bacteria, which has become a global public health problem.[1,2] Due to their unique structures, infections caused by Gram-negative bacteria and drug-resistant bacteria have gradually become the most intractable problems in clinical settings.[3,4] Although new drugs targeting Gram-positive bacteria have made significant progress in clinical trials, the special structure of Gram-negative bacteria and their characteristically easy means of transmitting drug resistance have prevented the development of new drugs targeting these bacteria in the past 20 years.[3] Therefore, in the exploration of new antibacterial drugs, more attention should be paid to those targeting Gram-negative bacteria. In addition to research and development of molecular drugs and antibiotics,[3,5] sustainable efforts have been devoted to the design and fabrication of antibacterial nanomaterials. Recently, several antibacterial nanomaterials, such as metal nanomaterials,[6,7] matrix composites,[8] transition metal dichalcogenides,[9,10] and carbon nanomaterials,[11] have been fabricated as effective antimicrobial tools. However, current new antibacterial strategies have not been able to achieve a breakthrough, likely due to the need to combine excellent antibacterial ability with an understanding of the resistance mechanisms in a cost-effective manner.[12,13] Further in-depth research on antibacterial nanomaterials, particularly for Gram-negative bacteria, is still necessary.

[a] *Department of Pharmaceutical Analysis, School of Pharmacy, Fujian Medical University, Fuzhou 350122, China. E-mail: shweng@fjmu.edu.cn*
[b] *Department of Pharmacy, Fujian Medical University Union Hospital, Fuzhou, 350001, China. E-mail: hjy8191@163.com*
[c] *Department of Stomatology, The First Affiliated Hospital of Fujian Medical University, Fuzhou, 350005, China. E-mail: huanglings@163.com*

† Electronic supplementary information (ESI) available: Identification of bacteria *via* MS, bacterial inhibition curves, MIC of QCDs to clinical resistant bacteria, MIC comparison, stability of antimicrobial activity of QCDs, interaction of papain and QCDs, and MS identification of the colonies. See DOI: https://doi.org/10.1039/d3tb00889d

‡ Zhang and Wu contributed equally to this work.

Carbon dots (CDs) have attracted increasing attention due to their controllable preparation, modulated properties, low toxicity, and potential for wide applications in the biomedical field.[14–16] The optimization of synthetic methods and precursors is considered the main synthetic approach to obtain CDs suitable for use in various applications.[14,17] Therefore, in the face of antibacterial resistance, antibacterial materials based on CDs have received ever-increasing attention due to their advantageous structure–property relationships. By using a biomass source,[18] quaternary ammonium compounds,[19] and antibiotics,[20,21] specific CDs with considerable antibacterial activity have been prepared through controllable strategies and applied to specific infection models. These works showed that CDs have great potential as a promising tool for killing microorganisms. Although there exist reports that have demonstrated materials with acceptable antibacterial activity and have explored antibacterial mechanisms towards Gram-positive bacteria,[22–28] there is still a lack of evidence or specific research that proves the feasibility of creating CDs with enhanced antibacterial against Gram-negative bacterial infections activity that acts *via* a systemic drug delivery model.

Currently, there is a lack of reports that evaluate the effect of antibacterial CDs administered *via* injection on infectious conditions. Due to the advantages of controllable dosage, rapid absorption, and quick increase in blood drug concentration, injection is the most important way to treat bacterial infections in clinical settings. Evaluating the *in vivo* efficacy of drugs administered *via* injection on disease progression (*e.g.*, intravenous administration and intraperitoneal injection) is significant for systematically estimating the practical value and clinical application prospects of a treatment. In clinical settings, Gram-negative bacteria are common pathogens in abdominal infections, urinary tract infections, and acquired pneumonia.[1,29] Acute peritonitis is a common inflammation of the abdomen with exudation of fibrin, serum, inflammatory cells, and pus, which may be caused by bacterial infections and/or physical damage.[30,31] The treatment for peritonitis caused by *E. coli* still needs improvement to further reduce mortality rates and side effects.[32] Additionally, Gram-negative bacteria are prone to developing antimicrobial resistance (AMR), which can lead to severe conditions that threaten human life and health. Although some antibacterial nanomaterials, including carbon dots, have been developed to treat bacterial infections, further assessment of antibacterial nanomaterials against Gram-negative bacteria-induced infections, such as acute peritonitis, is required.

In this work (Scheme 1), quaternized carbon dots (QCDs) were prepared *via* a one-step melting method using anhydrous citric acid and dimethyldiallyl ammonium chloride as precursors. QCDs with a size distribution of about 2 nm exhibited a fluorescence emission at 475 nm under excitation at 345 nm and showed broad-spectrum bactericidal ability due to the presence of a quaternary ammonium moiety and an alkane chain. Moreover, the antibacterial efficacy of QCDs against Gram-negative bacteria, including *E. coli* and clinically resistant strains, was found to be significantly better than that of several other reported carbon nanomaterials.[22–25] The antibacterial mechanism of the QCDs against *E. coli*, used as a model organism for Gram-negative bacteria, was also investigated in detail. *In vivo* evaluation of QCDs administered *via* intraperitoneal injection against acute bacterial peritonitis caused by *E. coli* demonstrated their potential for antibacterial treatment and inflammation reduction in bacterial infections.

2. Experimental section

2.1 Reagents and apparatus

Anhydrous citric acid (CA) and dimethyl diallyl ammonium chloride (DDA) were purchased from Aladdin Industrial Corporation (Shanghai, China). Mueller–Hinton (MH) broth was provided by Qingdao Hope Bio-technology Co., Ltd (Qingdao, China), while Columbia blood agar medium (blood agar plate) was obtained from Jiangmen Caring Trading Co., Ltd (Jiangmen, China). Gentamicin sulfate was provided by Solarbio Reagent

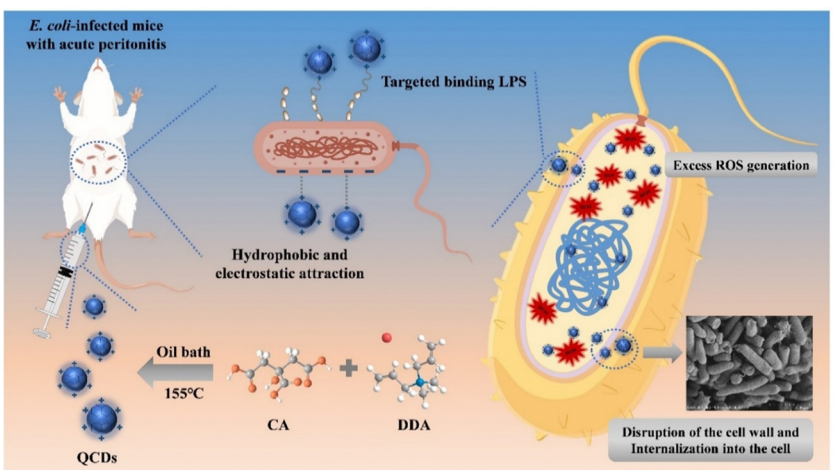

Scheme 1 Schematic representation of the synthesis of the QCDs, the antimicrobial mechanism, and the *in vivo* treatment of acute peritonitis using the QCDs.

Co., Ltd (Beijing, China), and cellulose dialysis bags (100–500) were provided by Shanghai Yuanye Bio-Technology Co., Ltd (Shanghai, China). The standard strains of *Staphylococcus aureus* (ATCC6538), methicillin-resistant *Staphylococcus aureus* (MRSA) (ATCC43300), *Escherichia coli* (ATCC25922), *Staphylococcus epidermidis* (ATCC12228), and *Serratia marcescens* (CMCC(B)41002) were purchased from Shanghai Luwei Microbial Sci. & Tech. Co., Ltd (Shanghai, China). Sample Pretreatment Reagents for Mass Spectrometry were provided by Autobio Diagnostics Co., Ltd (Zhengzhou, China), while HeLa and HaCat cells were obtained from Cobioer Biosciences Co., Ltd (Nanjing, China). All reagents were used without any further purification, and all aqueous solutions used in this work were prepared from ultrapure water.

Fluorescence spectra were measured using a Cary Eclipse fluorescence spectrophotometer (Agilent Technologies, Inc.). Absorption spectra were obtained using a UV-Vis spectrophotometer (UV-2450, Shimadzu Corporation, Japan). The zeta potentials were monitored using a Litesizer 500 nm laser particle size analyzer (Anton Paar GmbH, Austria). Transmission electron microscopy (TEM) and scanning electron microscopy (SEM) images were obtained using HT7800 (Hitachi) and SU8100 (Hitachi) microscopes, respectively. An automatic microbial mass spectrometry detection system (AUTOF MS1000, Zhengzhou Autobio Diagnostics Co., Ltd, China) was used for bacterial identification.

2.2 Preparation of QCDs

In a 50 mL round-bottom flask, 0.2 g of anhydrous citric acid was heated at 155 °C until completely melted. Then, 2 mL of 60% aqueous solution of DDA was added, and the reaction was continued for 210 min. After cooling, 10 mL of ultrapure water was added to dissolve the product. Next, the above solution was transferred into a cellulose dialysis bag (100–500 D) for dialysis treatment. The deionized water was replaced every 2 hours for a total of 6 times. Finally, the liquid in the dialysis bag was freeze-dried to obtain solid QCDs. The solid QCDs were stored at 2–8 °C for later use.

2.3 Culture and preparation of bacterial solutions

All types of bacteria were cultured on a blood agar plate using the flat line method in a biochemical incubator at 37 °C until a single colony was obtained. The single colony was then picked and inoculated into sterilized saline to form a bacterial suspension. The suspension with an OD_{600} value of 0.1 was defined as the 1.5×10^8 CFU mL^{-1} bacterial suspension for subsequent experiments.

2.4 Testing the antimicrobial activity of QCDs

The minimum inhibitory concentrations (MIC) of the QCDs against different tested bacteria were confirmed by a constant broth dilution test in 11 selected sterile test tubes.[23] One mL of MH broth was added to each test tube, except for the first tube. The first and second test tubes received 1 mL of the highest concentration of QCDs, and 1 mL of solution from the second test tube was added to the third test tube. This process was repeated until the 11th test tube was filled (which was then discarded). Blank broth and test bacterial pairs were set up. The blank bacterial suspension was adjusted to 1.5×10^8 CFU mL^{-1}. The tested bacterial solution was diluted 100 times with MH broth, and then 1 mL was taken and added into the test tube of QCDs with various concentrations. The tubes were incubated at 37 °C for 16–20 h, and the lowest concentration tube without bacterial growth was identified as the MIC of QCDs for the tested bacteria.

2.5 Antibacterial stability of the QCDs against *E. coli* in protein and serum

The antibacterial stability of QCDs in proteolytic proteins was assessed by measuring the MIC of QCDs against *E. coli* after treatment with trypsin, proteinase K, and papain (20 mg mL^{-1}, Sangon Biotech) at 37 °C. The antibacterial stability of QCDs in serum was assessed by determining the MIC of QCDs against *E. coli* in MH broth containing 50% FBS or 50% rabbit serum. The testing of the MIC was the same as the procedure illustrated in Section 2.4.

2.6 SEM characterization of the bacteria interacted by QCDs

E. coli and *S. aureus* samples with concentrations of 10^7–10^8 CFU mL^{-1} were incubated separately with 2 mg mL^{-1} of QCDs overnight. The samples were then centrifuged at 3000 rpm for 15 minutes at 4 °C. After washing, the sediment was fixed with electron microscopy fixative for 2 hours and then transferred at 4 °C for preservation and transportation. The fixed samples were washed with 0.1 M PBS (pH 7.4) three times for 15 minutes each. The samples were then fixed with 1% osmium in 0.1 M PBS at room temperature for 2 hours in the dark. Subsequently, the fixed samples were rinsed 3 times with 0.1M PBS and dehydrated using a series of alcohol concentrations (30%–50%–70%–80%–90%–95%–100%–100%) and isoamyl acetate for 15 minutes per step. Finally, the samples were dried in a critical point dryer. The dried samples were attached to a conductive carbon film double-sided adhesive and placed on the Au ion sputtering instrument for 30 seconds. The samples were evaluated using SEM.

2.7 CLSM characterization of the bacteria interacted by QCDs

E. coli and *S. aureus* samples with concentrations of 1.5×10^8 CFU mL^{-1} were incubated separately with 500 μg mL^{-1} of QCDs for 2 hours. The samples were centrifuged at 3000 rpm for 15 min at 4 °C and washed once with saline, then the bacteria were resuspended in saline and observed using confocal laser scanning microscopy (CLSM).

2.8 Changes in the zeta potential of bacteria interacting with QCDs

E. coli and *S. aureus* samples with concentrations of 1.5×10^8 CFU mL^{-1} were incubated with 1.5 mgmL^{-1} of QCDs at 37 °C for 4 h, respectively. The samples were centrifuged at 3000 rpm for 15 min at 4 °C, the supernatant was discarded, and the precipitate was washed three times with saline. The precipitate was resuspended in saline and the zeta potential was measured using a laser particle size analyzer.

2.9 Effects of LPS and cations on antibacterial stability of QCDs to *E. coli*

The effect of lipopolysaccharide (LPS) on the antibacterial activity of QCDs was evaluated using a constant broth dilution method. In brief, LPS from *E. coli* O111: B4 (Sigma, catalog number L2630) (8 μg mL^{-1}, 16 μg mL^{-1}, and 32 μg mL^{-1}) and QCDs at different concentrations were added to MH medium. Subsequently, 1 mL of *E. coli* broth dilution (1.5×10^6 CFU mL^{-1}) was added to the mixture. After incubation at 37 °C for 18 h, the MIC of QCDs at different concentrations of LPS were recorded. In addition, the effect of adding various cations, including NaCl, KCl, $CaCl_2$, $ZnCl_2$, and $MgCl_2$ (50 μg mL^{-1}), on the antibacterial activity of QCDs against *E. coli* was determined.

2.10 Treatment of mice with peritonitis using the QCDs

Animal experiments were conducted in accordance with the guidelines for animal experiments and were approved by the Ethical Committee of Experimental Animals of Fujian Medical University (Ethical number: IACUC FJMU 2022-0009). All clean-grade ICR mice ("mice") used in the experiment were purchased from the Experimental Animal Center of Fujian Medical University (Production License No.: SCXK (Fujian) 2016-0002) and were reared in a laboratory environment for three days, with access to water.

Thirty-six mice weighing 20 ± 4.5 g were randomly divided into three groups: a negative control group (n = 12), experimental group (n = 12), and positive control group (n = 12). Peritonitis was induced in the mice by administering 3.0×10^8 CFU mL^{-1} of *E. coli* suspension at 0.2 mL/10 g. The mice with peritonitis were treated with intraperitoneal injection. The experimental group and the positive control group were given QCDs solution (250 μg mL^{-1}) and gentamicin solution (100 μg mL^{-1}) at a dose of 0.1 mL/10 g, respectively. The negative control group was given the same dose of sterilized normal saline, once every 12 h. The mice were treated continuously for 72 h (3 d), during which the physiological conditions and mortality of the mice were observed. After 72 h of treatment, blood and organs were collected from each group of mice to evaluate the therapeutic effect of the QCDs.

2.11 *In vitro* cytotoxicity test for QCDs

The cytotoxicity of the QCDs was determined using the standard MTT assay. HaCat, MC3T3-E1, and HeLa cells were seeded in 96-well plates at a density of 4×10^3 cells per well, respectively. After 24 h of culture, 100 μL of different concentrations of QCDs (0, 31.25, 62.5, 125, 250, 500 μg mL^{-1}) were mixed with the cell culture medium and added to the cells. After culturing for 24 h, respectively, the cells were further cultured in medium containing 0.5 mg mL^{-1} MTT for 4 h. Finally, the medium was replaced with 150 μL of dimethyl sulfoxide (DMSO). The 96-well plate was shaken for 15 min at room temperature, and the optical density (OD) was measured at 490 nm using a microplate reader.

2.12 Statistical analysis

All experiments in this work were repeated three times, and the data were expressed as the mean ± standard deviation (SD). Statistical comparisons were analyzed by one-way ANOVA followed by Tukey's multiple comparisons tests using the GraphPad Prism 8 software. The level of significance was set at $P < 0.05$. The results were expressed as not significant (ns) for $P > 0.05$, and the level of significance was indicated by asterisks, where $^{****}P < 0.0001$.

3. Results and discussion

3.1 Characterization of QCDs

The morphology of the QCDs was investigated, and the results are shown in Fig. 1(A). The average particle size of the QCDs was centered at 2.0 nm with a range of 1.2 nm to 3.0 nm, suggesting a uniform size distribution. The lattice parameter was 0.24 nm (Fig. 1(A) HRTEM (down)), which is consistent with the structure of graphitic carbon.[33] Moreover, the optical properties of the QCDs were evaluated using UV-visible absorption and fluorescence spectroscopy. As shown in Fig. 1(B), the QCDs have a main

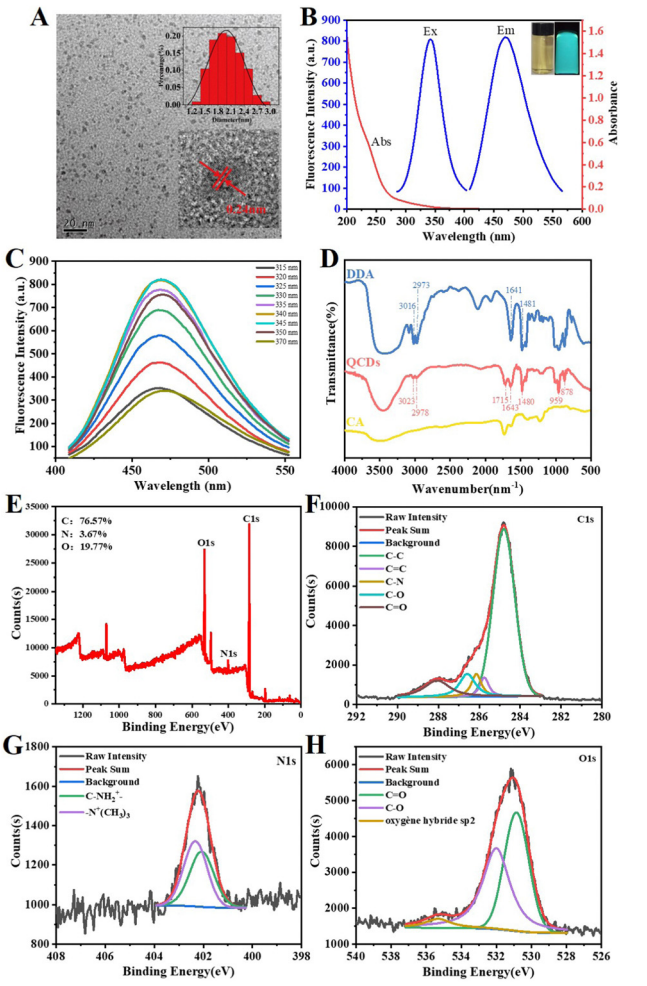

Fig. 1 Characterizations of the QCDs. (A) TEM image and particle size distribution (inset up) and HRTEM image (inset down). (B) UV-vis spectra and fluorescence spectra. (C) Fluorescence emission spectra. (D) FTIR spectrum of the QCDs. (E) XPS spectrum. (F)–(H) High-resolution XPS C1s, N1s, and O1s spectra.

absorption peak at 245 nm ascribed to the π–π* transition of the sp^2 hybrid orbital of C=C. Correspondingly, the maximum fluorescence emission at 475 nm was obtained when the excitation wavelength was 345 nm (blue line in Fig. 1(B)). As can be seen from the inset of Fig. 1(B), the obtained QCDs solution appeared light yellow and transparent under sunlight and exhibited blue fluorescence under ultraviolet light irradiation (365 nm). Furthermore, when changing the wavelength at which the QCDs were excited, the maximum emission wavelength remained unchanged at 475 nm whilst the fluorescence intensity was altered (Fig. 1(C)). This behavior indicates that the QCDs show excitation-independent fluorescence behavior. The optical properties of the QCDs also revealed features typical of carbon dots.[15,16]

Fourier-transform infrared (FTIR) spectroscopy was used to characterize the functional groups of the QCDs, as shown in Fig. 1(D). The absorption peaks of DDA at 3016 cm^{-1}, 2973 cm^{-1}, and 1641 cm^{-1} were attributed to the C–H single bond asymmetric stretching vibration (ν^{as}), the C–H single bond symmetric stretching vibration (ν^{s}), and the C=C stretching vibration, respectively.[22] After DDA reacted with citric acid, the generated QCDs showed peaks at 3023 cm^{-1} and 2978 cm^{-1} corresponding to the asymmetric stretching vibration (ν^{as}) and symmetric stretching vibration (ν^{s}) of C–H, respectively, suggesting the presence of long alkane chains in the QCDs. The weakened absorption for C–H may be due to the relatively low content of alkane chains in the QCDs compared to DDA. The presence of long alkane chains may impart the property of hydrophobicity to the QCDs.[34] The absorption peak at 1715 cm^{-1} was attributed to the C=O stretching vibration (ν), while the QCDs absorption peak at 1643 cm^{-1} was attributed to the C=C stretching vibration (ν). The QCDs absorption peak at 1480 cm^{-1} was ascribed to the shear in-plane bending vibration (δ) of the C–H connected to the ($-N^{+}(CH_3)_3$) (quaternary ammonium group). This value is consistent with the C–H absorption peak at 1481 cm^{-1} in DDA, confirming the presence of the quaternary ammonium groups on the QCDs. Moreover, the QCDs absorption peaks at 959 cm^{-1} and 878 cm^{-1} might be caused by the C–C and C–O stretching vibrations (ν), respectively. X-ray photoelectron spectroscopy (XPS) was used to further determine the molecular composition of the QCDs. The full range XPS spectrum suggested that the percentage content of C, N, and O in the QCDs was 76.57%, 3.67%, and 19.77% (Fig. 1(E)), respectively. The high-resolution C1s XPS spectra (Fig. 1(F)) had two peaks at 284.8 eV and 285.75 eV, which were assigned to the C–C/C=C groups of graphene carbon. Furthermore, the other three peaks at 286.15 eV, 286.58 eV, and 288.07 eV were attributed to C–N (sp^3 hybrid carbon), C–O (sp^3 hybrid carbon), and C=O, respectively. The high-resolution N1s XPS spectrum (Fig. 1(G)) was deconvoluted to pyridine C–N–C (402.07 eV) and $-N^{+}(CH_3)_3$ (402.32 eV), respectively, suggesting the doping of N in the form of pyridine nitrogen and quaternary ammonium nitrogen. In addition, the quaternary ammonium nitrogen content was higher than that of pyridine nitrogen according to the peak area integrals. The zeta potential of the QCDs was found to be positive (+11.3 mV) in saline (Fig. 4(A)), which could be attributed to the presence of quaternary ammonium groups on the surface. The O1s XPS spectra (Fig. 1(H)) had a peak at 530.85 eV for the C=O of carbonyl oxygen, at 532 eV for C–O, and at 535.32 eV for the sp^2 hybridized oxygen. Overall, the FTIR and XPS characterization results indicate the presence of quaternary ammonium groups ($-N^{+}(CH_3)_3$), carbonyl groups (C=O), and typical graphene carbon in the QCDs.

3.2 Antibacterial activity of QCDs *in vitro*

The activity of the QCDs against bacteria, especially Gram-negative bacteria, was investigated through the evaluation of the MICs. Using a standard broth dilution test, the MIC results for the QCDs against general bacteria and resistant bacteria were measured. As shown in Table 1, the QCDs exhibited an MIC of 30 μg mL^{-1} against Gram-negative bacteria, *E. coli*, and *S. marcescens*. Moreover, the QCDs also exhibited bactericidal capacity against the common Gram-positive bacteria *S. aureus*, *S. epidermidis*, and MRSA, with an MIC of 15 μg mL^{-1}, suggesting broad-spectrum antibacterial activity of QCDs. Compared with the MIC of gentamicin against standard strains of bacteria, the MIC of the QCDs was higher. Meanwhile, the MIC of gentamicin against MRSA was significantly increased. The MIC of the QCDs against resistant bacterium (MRSA) was the same as the MIC against non-resistant bacteria. This result demonstrates the superior performance of the QCDs against resistant bacteria. Furthermore, the antibacterial activity of the QCDs against clinically drug resistant *E. coli* was evaluated. The results (Table S2, ESI†) implied that the QCDS have strong antibacterial activity against resistant Gram-negative bacteria. Moreover, compared with other reported antibacterial carbon dots (Table S3, ESI†),[22–28] the MIC value of the QCDs against *E. coli* was smaller than that of other carbon dots, suggesting that the QCDs possessed enhanced antibacterial activity against Gram-negative bacteria.

A microdilution broth method was used to study the inhibition of *E. coli* and *S. aureus* by the QCDs by measuring the OD_{600} value of the culture medium after the bacteria were treated with different concentrations of QCDs at different time intervals, as shown in Fig. S1 (ESI†). The post-antibiotic effect (PAE) following exposure of the bacteria to the QCDs was observed in selected bacteria, resulting in delayed regrowth during the initial periods.[35] As shown in Fig. S1 (ESI†), the OD_{600} values gradually decreased as the concentration of the QCDs increased, indicating concentration-dependent antibacterial ability. *E. coli* was completely suppressed in the broth medium at a concentration of 30 μg mL^{-1} within 24 h, and the antibacterial effect of the QCDs on bacteria at the MIC was observed for up to 40 h or longer.

Table 1 MICs of the QCDs and gentamicin against bacteria

Bacterial strain	Number	G^+/G^-	MIC of QCDs (μg mL^{-1})	MIC of gentamicin (μg mL^{-1})
E. coli	ATCC25922	G^-	30	2
S. marcescens	CMCC(B)41002	G^-	30	1
S. aureus	ATCC6538	G^+	15	1
MRSA	ATCC43300	G^+	15	60
S. epidermidis	ATCC12228	G^+	15	0.1

The effect of three proteases and two kinds of serum on the antibacterial activity of the QCDs was studied, as shown in Fig. S2 (ESI†). The MIC of the QCDs was maintained after incubation with 20 mg mL^{-1} of trypsin, proteinase K, 50% fetal bovine serum (FBS), and 50% rabbit serum at 37 °C for 12 h, suggesting that the QCDs possess stable antibacterial activity free from the possible interference from digestive enzymes or other biological components. Meanwhile, the MIC of the QCDs in the presence of papain was double. Papain has its own intrinsic fluorescence due to the presence of aromatic amino acid residues.[36,37] The interaction of these aromatic amino acid residues and the nanoparticles will induce the quenching of the fluorescence of papain.[36,37] As shown in Fig. S3 (ESI†), under 280 nm excitation, papain had a strong optimal emission peak at 340 nm. After the introduction of QCDs, the fluorescence intensity of papain at 340 nm decreased significantly, indicating the interaction between the QCDs and papain. The interaction between the QCDs and papain creates competition for the interaction of the QCDs and the bacteria, resulting in the inhibition of the antibacterial activity of the QCDs. Generally speaking, the low impact of common proteases and serum on the antibacterial activity of the QCDs will enable the potential effectiveness of QCDs for further antibacterial applications, like treating *in vivo* infections.

3.3 Antibacterial mechanism of the QCDs

SEM was applied to investigate the integrity of the bacterial cell membrane of *E. coli* and *S. aureus* before and after interaction with the QCDs. As shown in Fig. 2, the bacterial cells of *E. coli* and *S. aureus* were morphologically intact and clearly visible before treatment with the QCDs. After incubation with the QCDs, damage and several defects appeared on the cell surface of the *E. coli* with some scattered fragments. Similarly, the surface of *S. aureus* treated with the QCDs was no longer smooth and round, and some bacterial cells were incomplete. SEM results showed that the QCDs caused physical or mechanical damage to the microbial cell wall or outer membrane, resulting in overall physiological dysfunction of the bacteria and ultimately bacterial death.

CLSM was used to verify the possible attachment of the QCDs to bacterial cells based on the fluorescence properties of the QCDs. As shown in Fig. 3(A), *S. aureus* and *E. coli* show bright blue fluorescence under excitation after incubation with the QCDs, indicating that the QCDs could effectively stain the bacterial cells through adsorption. The difference in the fluorescence intensity of stained *S. aureus* and that of *E. coli* was statistically significant (Fig. 3(B)), suggesting that the QCDs adhered more to *S. aureus*. The ability of the QCDs to adhere differently to various bacteria may induce different inhibitory effects on different bacteria. However, considering that the primary condition for an antibacterial effect is to enhance the adsorption or fixation of drugs on bacteria,[13,38] the antibacterial performance of the QCDs against Gram-negative bacteria was significantly improved compared to previous works.[22–25] The mode of action of the QCDs on Gram-negative bacteria was further investigated to evaluate the mechanism of its enhanced antibacterial ability against Gram-negative bacteria.

Electrostatic interactions between the positively charged nanoparticles and the negatively charged bacterial cell membrane result in the perforation and rupture of the cell membrane, leading to an antibacterial effect on the bacteria.[39] The positively

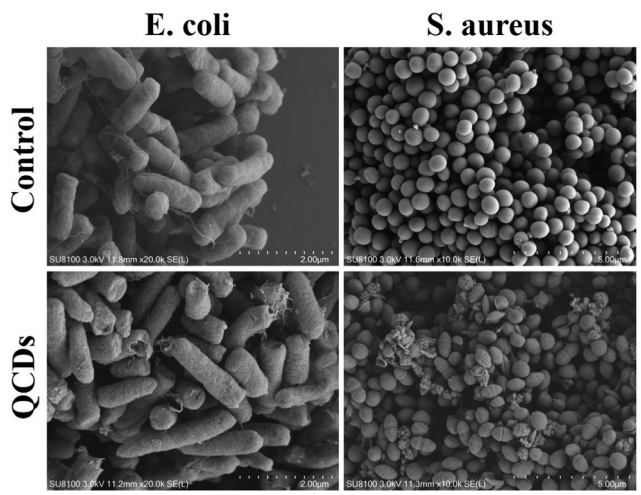

Fig. 2 SEM images of *E. coli* and *S. aureus* without or with QCDs treatment.

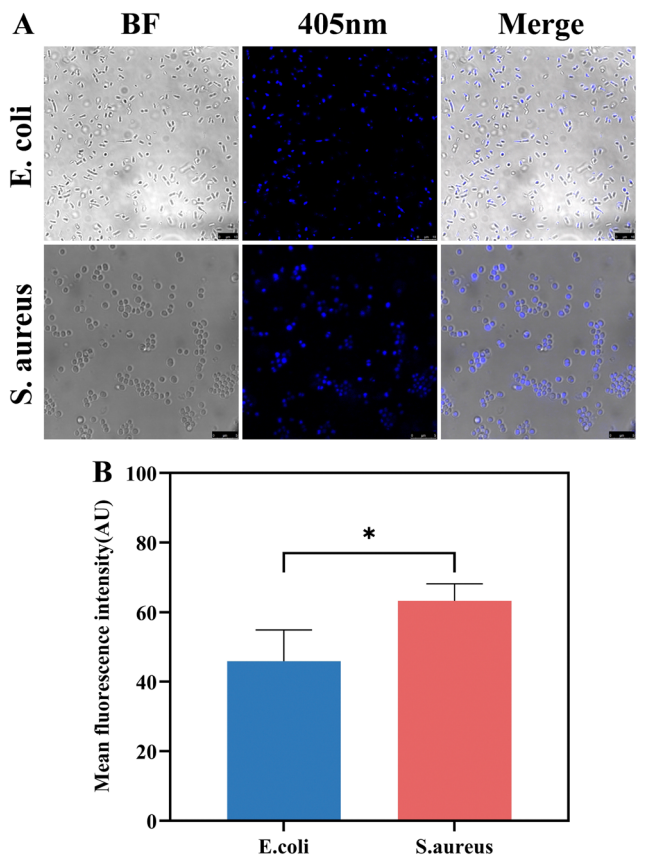

Fig. 3 Interaction of the QCDs with *E. coli* and *S. aureus*. (A) CLSM images. (B) Quantitative fluorescence analysis of the CLSM images obtained following excitation at 405 nm (*$P < 0.05$).

charged surface of antimicrobial materials is significant because most bacterial cell walls, of which phosphatidylethanolamine is the main component (70%), are negatively charged. As shown in Fig. 4(A), the zeta potential of *E. coli* was −20.6 mV. After adding the positively charged QCDs (with a zeta potential of +11.4 mV), the zeta potential of the mixture of QCDs and *E. coli* was 1.3 mV, indicating the presence of an electrostatic interaction between the QCDs and *E. coli*. In contrast, the zeta potential of the interaction between the QCDs and *S. aureus* was +9.0 mV. The lower zeta potential of the QCDs and *E. coli* system suggested some other interaction between the QCDs and *E. coli* besides electrostatic interactions.

In order to further understand absorption of the QCDs on the outer membrane of Gram-negative bacteria, the possible interaction between the QCDs and LPS was investigated. This approach was selected because LPS is an abundant component in the cell membrane of Gram-negative bacteria. Using *E. coli* as a model, the MIC of the QCDs was found to gradually increase as an increased amount of exogenously purified LPS from *E. coli* was added. This result illustrated LPS-dose-dependent antibacterial activity of QCDs with respect to *E. coli* (Fig. 4(B)), suggesting a strong interaction between the QCDs and LPS, similar to that of LPS-targeting antibiotics.[40,41] We further investigated whether the QCDs bind to the negatively charged domain of lipid A in the LPS. The effects of five common cations on the antibacterial activity of the QCDs were compared, as shown in Fig. 4(C). Ca^{2+} significantly

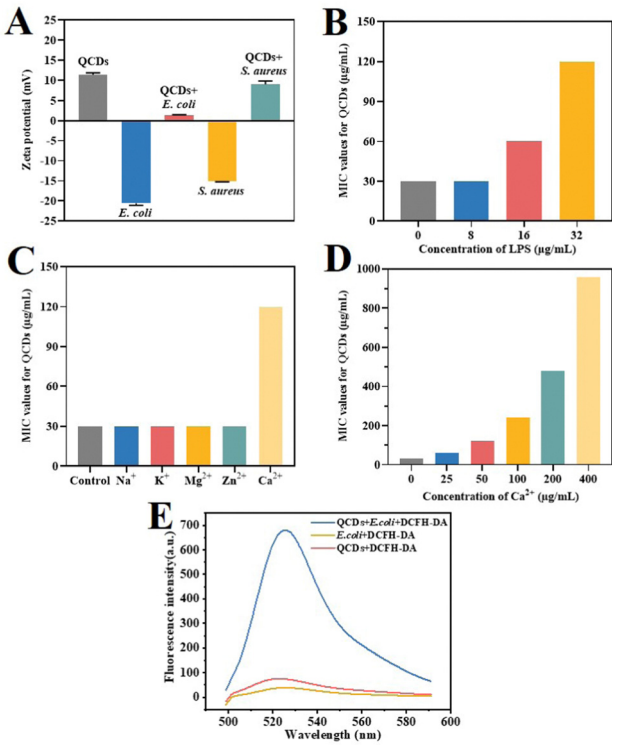

Fig. 4 Antibacterial mechanism of the QCDs. (A) The zeta potentials of different interacting systems in saline. (B)–(D) The influence of LPS, metal cations, and Ca^{2+} on the antibacterial activity of the QCDs. (E) Fluorescence spectra of the QCDs and intercellular ROS generation in *E. coli* using DCFH-DA as a probe (n = 3).

inhibited the antibacterial activity of the QCDs. Subsequently, the effects of different concentrations of Ca^{2+} on the antibacterial activity of the QCDs implied that Ca^{2+} had a dose-dependent inhibitory effect on the antibacterial activity of the QCDs (Fig. 4D). Since the lipid A molecules in LPS can be neutralized by a divalent ion bridge through electrostatic interactions to achieve tight accumulation and low permeability,[42] the inhibitory effect of Ca^{2+} on the antibacterial activity of the CQDs confirmed the interaction of the QCDs with lipid A. The combination of the presence of a positive charge and hydrophobicity on the QCDs, the interaction between the QCDs and LPS, and the inhibition of Ca^{2+} on the antibacterial activity of QCDs implied that the QCDs act on Gram-negative bacteria due to their hydrophobic properties and electrostatic action on the cell membrane of Gram-negative bacteria. This dual action will promote the absorption of the QCDs into bacteria, increasing the permeability of the bacterial cell membrane, causing leakage of intracellular substances, and leading to changes in the morphology of bacterial cells that kill the bacteria.

The antibacterial effect mainly depends on the interaction of the antibacterial drugs entering the bacterial cells and bacterial sub-organs. Using DCFH-DA as a probe, the possible production of reactive oxygen species (ROS) in bacterial cells was investigated, as shown in Fig. 4(E). Almost no fluorescence was detected at 525 nm during the interaction between DCFH-DA and *E. coli*, and the interaction of DCFH-DA with the QCDs. The addition of the QCDs excited the DCFH-DA and *E. coli* system with evident fluorescence observed at 525 nm, indicating that the interaction of the QCDs with the bacterial cells stimulated the production of ROS, which have an antibacterial and even bactericidal effect.

3.4 Biosafety of the QCDs

The potential cytotoxicity of the QCDs was investigated using HaCat, MC3T3-E1, and HeLa cells as models. As shown in Fig. 5(A)–(C), at a concentration of 62.5 μg mL^{-1}, the survival rates of the three cells were higher or close to 80% after 24 h of treatment. When the concentration of the QCDs reached 250 μg mL^{-1}, the survival rates of the HaCat and MC3T3-E1 cells were higher than 70% after 24 h of treatment. Meanwhile, the survival rate of the HeLa cells was lower than that of the two other cell types. Considering that the MIC of the QCDs against most bacteria was lower than or equal to 30 μg mL^{-1}, it suggested that the biosafety of the QCDs at the concentration required for effective antibacterial action would be greatly improved in practice.

A hemolysis test was performed using red blood cells according to a standard method.[16] As shown in Fig. 5(D), the solution turned red following centrifugation when red blood cells were dispersed in sterilized water. This was due to the different osmotic pressure inside and outside the cells in pure water. Correspondingly, the red blood cells were found to be well dispersed in different concentration physiological saline solutions of QCDs. After centrifugation, the centrifuge tube contained the deposited red blood cells and a transparent and almost colorless solution. Even when the concentration of the QCDs reached 500 μg mL^{-1}, the hemolysis rate was less than

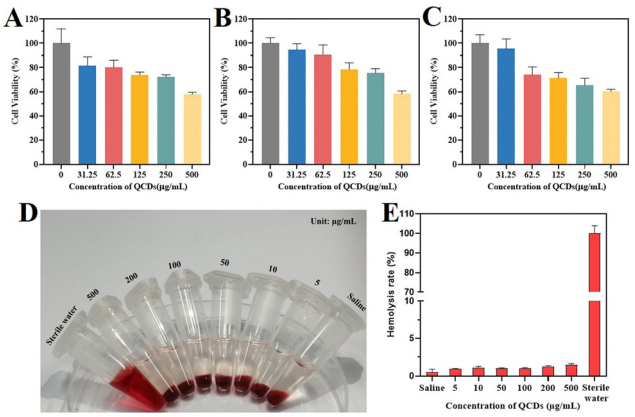

Fig. 5 Biosafety of the QCDs. (A)–(C) The survival rate of HaCat, MC3T3-E1, and HeLa cells treated with QCDs for 24 h. (D) and (E) Photograph of hemolysis study samples and graph showing hemolysis rate of the QCDs (n = 3).

5% compared to the dispersion of red blood cells in water (Fig. 5(E)), suggesting that the QCDs did not rupture red blood cells under physiological conditions.

3.5 Treatment of infectious acute peritonitis using the QCDs

The *in vivo* efficiency of the QCDs for the treatment of acute peritonitis caused by *E. coli* was evaluated. A mouse model of infectious acute peritonitis was induced by injecting mice with 3.0×10^8 CFU mL^{-1} *E. coli*. A negative control group (Modeling), an experimental group (QCDs), and a positive control group (Gentamicin) were intraperitoneally injected with normal saline, 250 μg mL^{-1} of QCDs, and 100 μg mL^{-1} of gentamicin at a dose of 0.1 mL/10 g, respectively. Fig. 6(A) shows that 100% of the mice in the negative control group died within 72 h after being given only normal saline, while the survival rate of the recovered mice treated with QCDs in the experimental group was the same as that in the positive control group (75%). This indicates that 250 μg mL^{-1} of QCDs could effectively increase the survival rate of the mice with acute peritonitis, showing a therapeutic effect similar to that of gentamicin.

Blood samples were collected from the healthy mice (blank) and the different groups. The number of white blood cells (WBC) and neutrophils (NEUT) in the blood of the different mice were measured to evaluate the effect of the QCDs on the regression of infection, as shown in Fig. 6(B) and (C). The results show that the levels of WBC and NEUT in the blood of the blank group were the lowest, while the levels of WBC and NEUT in the blood was obviously higher in the modeling group, representing a statistically significant difference. After treating with QCDs and gentamicin for 72 h, the levels of WBC and NEUT in the blood of the mice in the experimental and positive control groups were significantly decreased and close to the levels of healthy mice. This suggests that treatment with the QCDs effectively reduces the levels of WBC and NEUT in the mice, allowing the inflammation to subside.

Based on clinical diagnostic guidelines, magnetic resonance imaging (MRI) was further performed to compare the abdominal cavity of the mice in the different groups. As shown in Fig. 6(D), in the blank group, the T2 fast spin-echo (fs) images

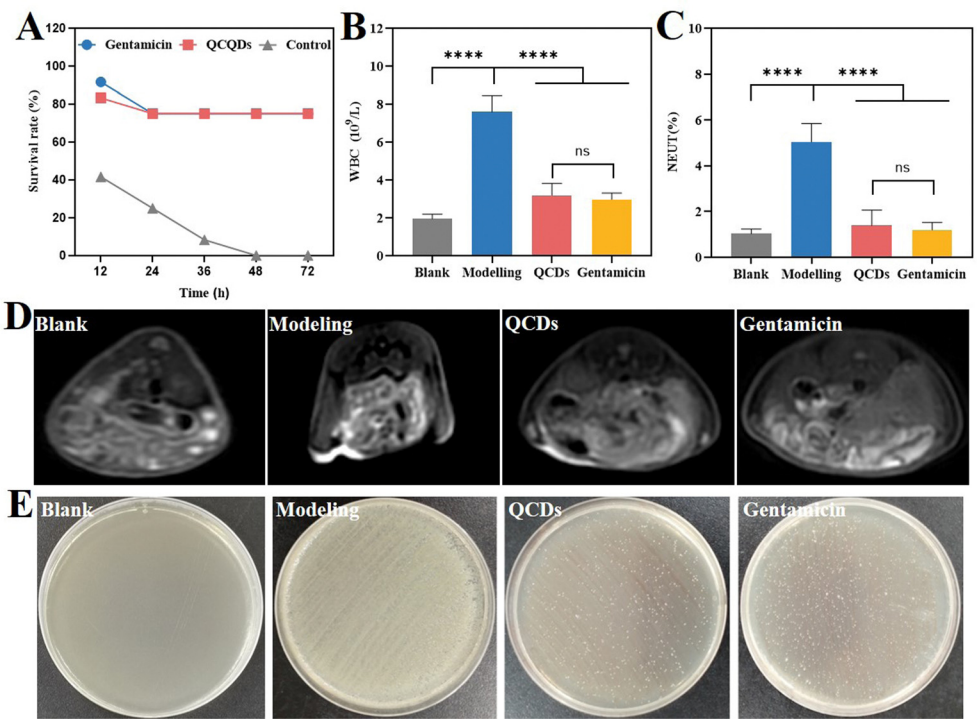

Fig. 6 *In vivo* antimicrobial properties of the QCDs. (A) The survival rates. (B) and (C) Levels of WBC and NUET in the mice blood samples. (D) MRI images. (E) Bacterial smear plates for each blood sample (****$P < 0.0001$).

of the intestinal wall had a low signal, and the interintestinal space was clear, suggesting a normal abdominal cavity associated with healthy mice. In the negative control group, the T2 fs images of the intestinal wall of the mice had a high signal, and abdominal dropsy was observed. The T2 fs images of the intestinal wall of mice in the experimental and positive control groups showed a low signal, the interintestinal space was clear and similar to the blank group, and no abdominal dropsy was found in the mice. The MRI results indicated that the QCDs effectively treated the mice with acute peritonitis, alleviating abdominal infection and achieving inflammation regression, suggesting that the QCDs had the same therapeutic effect as gentamicin sulfate.

After 72 hours of intervention, the blood of the mice in the blank, negative control, experimental, and positive control groups were evenly smeared on an agar plate to evaluate the *in vivo* residual bacteria, as shown in Fig. 6(E). No colonies grew on the agar plates of the blank group. In the negative control group, very dense colonies of bacteria grew on the agar plates, which may be due to the overabundance of bacteria or the low immune function of the mice resulting in the spread of infection to form diffuse peritonitis. Furthermore, the identification of the bacterial colonies of the negative control group was performed using MALDI-TOF MS, as shown in Fig. S4 (ESI†). Compared with a standard spectrum, the colonies were identified to be *E. coli*, suggesting that *E. coli* had spread in the modeling mice. It implied that bacteria and toxins in the peritoneal exudates (Fig. 6(D)) of the modeling mice are absorbed by the peritoneum and then enter the blood through

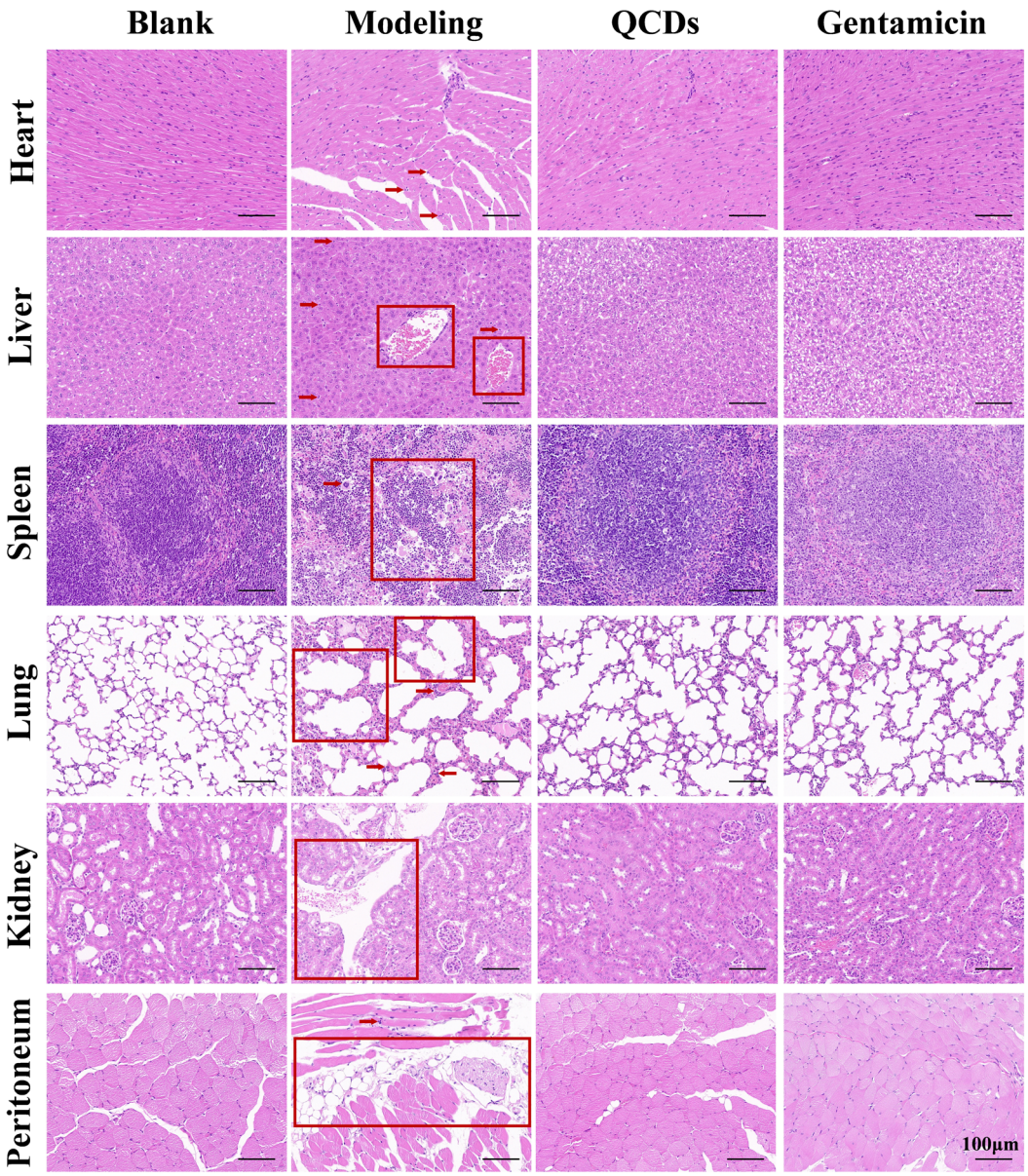

Fig. 7 HE-stained sections of the major organs of each group of mice (red arrows and red boxes indicate inflammatory cells and sites of inflammation, respectively).

lymphatic vessels, causing a series of symptoms. The colony of the experimental group was similar to that of the positive control group in the survival mice. Among the 9 recovered mice of each treated group, the blood samples from 7 mice found almost no colonies after following the same incubation process. Compared with the negative control group, the number of colonies on the agar plates of the other two blood samples from the two treated groups were significantly reduced and sparse (Fig. 6(E)), suggesting that the QCDs exerted *in vivo* antibacterial effects comparable to those of gentamicin.

Pathological analysis of the heart, liver, spleen, lung, kidney, and peritoneum of each group of mice was carried out using hematoxylin and eosin (HE) staining. As shown in Fig. 7, compared to the blank group, the modeling group showed different inflammatory responses in different organs. For example, a small number of infiltrating lymphocytes and neutrophil granulocytes are found in the heart, some infiltrating lymphocytes and neutrophil granulocytes are seen in the portal area of the liver with severe swelling and balloon-like hepatocytes, a damaged lymphoid follicle structure with extramedullary hematopoiesis is found in the spleen, peribronchitis as well as alveolar fusion, septal dilatation, and congestion are seen in the lung, whilst renal tubule dilatation is seen in the kidneys. In addition, stromal fibrous proliferation with infiltration of some lymphocytes and neutrophil granulocytes was also observed in the negative control mice after *E. coli* infection. In conclusion, all the above histopathological changes indicated that acute peritonitis leads to severe inflammatory responses in all organs in the negative control mice. However, compared to the negative control mice, the experimental and positive control mice showed little infiltration and histopathological changes in the organs, similar to healthy mice. This indicates that QCDs can promote the recovery and healing of peritonitis in mice.

The results of the routine analysis of blood, MRI, and bacterial culture and the pathological analysis of major organs suggested that QCDs had excellent performance in treating acute peritonitis caused by *E. coli*, with a curative effect similar to that of gentamicin. Furthermore, the advantage of using QCDs is that the QCDs can also treat resistant bacteria, implying that they have significant prospects for clinical application.

4. Conclusions

In summary, broad-spectrum antibacterial quaternized carbon dots (QCDs) with enhanced activity against Gram-negative bacteria were synthesized *via* an effective one-step method. The small-sized QCDs contained quaternary ammonium groups and long alkane chains, which enable them to strongly bind to the cell membrane (specifically lipopolysaccharide) of Gram-negative bacteria through electrostatic and hydrophobic effects. *In vitro* safety assessments implied the biocompatibility of the QCDs. *In vivo* experimental results showed that the QCDs and gentamicin sulfate had the same therapeutic effect on mouse models with *E. coli*-induced peritonitis. In addition to the general administration of antibacterial nanomaterials on wounds, this work further develops the use of carbon dots in the antibacterial field through an injection mode, thus expanding the range of clinical administration methods and applications that carbon dots have in medicine.

Author contributions

Xintian Zhang, Pingping Wu, and Xiaoli Hao: methodology, data curation, formal analysis, visualization, writing – original draft, writing – review & editing. Pingping Wu and Xiaoli Hao: methodology, data curation, formal analysis, visualization, writing – original draft. Jiamiao Liu, Zhengjun Huang, and Weifeng Chen: data curation, formal analysis. Shaohuang Weng: conceptualization, formal analysis, project administration, supervision, funding acquisition, writing – original draft, writing – review & editing. Lingling Huang and Jianyong Huang: project administration, funding acquisition, writing – review & editing.

Conflicts of interest

There are no conflicts to declare.

Acknowledgements

This work was financially supported by the National Science Foundation of Fujian Province (2021J01220, 2023Y0021), and Joint Funds for the Innovation of Science and Technology, Fujian Province (2019Y9068, 2021Y9007), and Fujian provincial health technology project (2021GGA011). The authors thank the Public Technology Service Center Fujian Medical University and its staff member Mr Zhihong Huang for their technical guidance and assistance on laser confocal microscope imaging in this work.

References

1 T. Krell and M. A. Matilla, *Microb. Biotechnol.*, 2022, **15**, 70–78.
2 J. M. An, S. Kang, C. W. Koh, S. Park, M. S. Oh and D. Kim, *Nanoscale Horiz.*, 2022, **7**, 873–882.
3 Y. Imai, K. J. Meyer, A. Iinishi, Q. Favre-Godal, R. Green, S. Manuse, M. Caboni, M. Mori, S. Niles, M. Ghiglieri, C. Honrao, X. Y. Ma, J. J. Guo, A. Makriyannis, L. Linares-Otoya, N. Böhringer, Z. G. Wuisan, H. Kaur, R. R. Wu, A. Mateus, A. Typas, M. M. Savitski, J. L. Espinoza, A. O'Rourke, K. E. Nelson, S. Hiller, N. Noinaj, T. F. Schäberle, A. D'Onofrio and K. Lewis, *Nature*, 2019, **576**, 459–464.
4 S. S. Jean, D. Harnod and P. R. Hsueh, *Front. Cell. Infect. Microbiol.*, 2022, **12**, 823684.
5 P. Zhou and J. Y. Hong, *Acc. Chem. Res.*, 2021, **54**, 1623–1634.
6 S. Cheeseman, A. J. Christofferson, R. Kariuki, D. Cozzolino, T. Daeneke, R. J. Crawford, V. K. Truong, J. Chapman and A. Elbourne, *Adv. Sci.*, 2020, **7**, 1902913.
7 A. Panáček, L. Kvítek, M. Smékalová, R. Večeřová, M. Kolář, M. Röderová, F. Dyčka, M. Šebela, R. Prucek, O. Tomanec and R. Zbořil, *Nat. Nanotechnol.*, 2018, **13**, 65–71.

8 Y. S. Tu, P. Li, J. J. Sun, J. Jiang, F. F. Dai, C. Z. Li, Y. Y. Wu, L. Chen, G. S. Shi, Y. W. Tan and H. P. Fang, *Adv. Funct. Mater.*, 2021, **31**, 2008018.

9 D. Q. Xu, X. J. He, E. Obeng, Z. Y. Ye, J. L. Shen and X. Ding, *Mater. Des.*, 2022, **223**, 111124.

10 J. Sahoo and M. De, *J. Mater. Chem. B*, 2022, **10**, 4588–4594.

11 Q. Xin, H. Shah, A. Nawaz, W. Xie, M. Z. Akram, A. Batool, L. Tian, S. U. Jan, R. Boddula, B. J. A. M. Guo, Q. Liu and J. R. Gong, *Adv. Mater.*, 2019, **31**, 1804838.

12 M. Abbas, M. Ovais, A. Atiq, T. M. Ansari, R. Xing, E. Spruijt and X. Yan, *Coord. Chem. Rev.*, 2022, **460**, 214481.

13 P. Li, L. Sun, S. Xue, D. Qu, L. An, X. Wang and Z. Sun, *SmartMater.*, 2022, **3**, 226–248.

14 B. Wang, H. Cai, G. I. Waterhouse, X. Qu, B. Yang and S. Lu, *Small Sci.*, 2022, **2**, 2200012.

15 W. D. Han, C. F. Miao, X. T. Zhang, Y. N. Lin, X. L. Hao, Z. J. Huang, S. H. Weng, X. H. Lin, X. Z. Guo and J. Y. Huang, *Anal. Chim. Acta*, 2021, **1179**, 338853.

16 R. Y. Cai, C. F. Miao, L. Zhang, Y. Zhou, Y. B. Liu, C. Zheng, W. D. Han, Z. J. Huang, X. Zhou and S. H. Weng, *Sens. Actuators, B*, 2022, **361**, 131721.

17 T. C. Wareing, P. Gentile and A. N. Phan, *ACS Nano*, 2021, **15**, 15471–15501.

18 M. Tariq, A. Singh, N. Varshney, S. Samanta and M. P. Sk, Biomass-derived carbon dots as an emergent antibacterial agent, *Mater. Today Commun.*, 2022, **33**, 104347.

19 X. Chu, P. Zhang, Y. Liu, B. Sun, X. Huang, N. Zhou, J. Shen and N. Meng, *J. Mater. Chem. B*, 2022, **10**, 2865–2874.

20 P. Li, S. Liu, W. Cao, G. Zhang, X. Yang, X. Gong and X. Xing, *Chem. Commun.*, 2020, **56**, 2316–2319.

21 L. N. Wu, Y. J. Yang, L. X. Huang, Y. Zhong, Y. Chen, Y. R. Gao, L. Q. Lin, Y. Lei and A. L. Liu, *Carbon*, 2022, **186**, 452–464.

22 C. F. Zhao, X. W. Wang, L. N. Wu, W. Wu, Y. J. Zheng, L. Q. Lin, S. H. Weng and X. H. Lin, *Colloids Surf., B*, 2019, **179**, 17–27.

23 X. L. Hao, L. L. Huang, C. F. Zhao, S. N. Chen, W. J. Lin, Y. N. Lin, L. R. Zhang, A. A. Sun, C. F. Miao, X. H. Lin, M. Chen and S. H. Weng, *Mater. Sci. Eng., C*, 2021, **123**, 111971.

24 C. F. Zhao, L. N. Wu, X. W. Wang, S. H. Weng, Z. P. Ruan, Q. C. Liu, L. Q. Lin and X. H. Lin, *Carbon*, 2020, **163**, 70–84.

25 J. Yang, G. Gao, X. Zhang, Y. H. Ma, X. Chen and F. G. Wu, *Carbon*, 2019, **146**, 827–839.

26 M. Yu, X. Guo, H. Lu, P. Li, R. Huang, C. Xu, X. Gong, Y. Xiao and X. Xing, *Carbon*, 2022, **199**, 395–406.

27 F. Lu, Y. Ma, H. Wang, M. Zhang, B. Wang, Y. Zhang, H. Huang, F. Liao, Y. Liu and Z. Kang, *Mater. Today Commun.*, 2021, **26**, 102000.

28 Z. Wang, L. Sheng, X. Yang, J. Sun, Y. Ye, S. Geng, D. Ning, J. Zheng, M. Fan, Y. Zhang and X. Sun, *Sustainable Mater. Technol.*, 2023, **36**, e00584.

29 S. Portsmouth, D. van Veenhuyzen, R. Echols, M. Machida, J. C. A. Ferreira, M. Ariyasu, P. Tenke and T. Den Nagata, *Lancet Infect. Dis.*, 2018, **18**, 1319–1328.

30 J. Ballus, J. C. Lopez Delgado, J. Sabater Riera, X. L. Perez Fernandez, A. Betbese and J. A. Roncal, *BMC Infect. Dis.*, 2015, **15**, 1–6.

31 D. Porner, S. Von Vietinghoff, J. Nattermann, C. P. Strassburg and P. Lutz, *Expert Opin. Pharmacother.*, 2021, **22**, 1567–1578.

32 J. Li, R. Cha, X. Zhao, H. Guo, H. Luo, M. Wang, F. Zhou and X. Jiang, *ACS Nano*, 2019, **13**, 5002–5014.

33 Q. Hu, Y. Fang, Z. Du, Z. L. Guo, Z. Y. Liu, Y. Huang, J. Lin and C. C. Tang, *Carbon*, 2021, **182**, 134.

34 C. Chen, S. Tao, X. Qiu, X. Ren and S. Hu, *Carbohydr. Polym.*, 2013, **91**, 269–276.

35 L. D. Saravolatz, J. Pawlak, H. Martin, S. Saravolatz, L. Johnson, H. Wold, M. Husbyn and W. M. Olsen, *Lett. Appl. Microbiol.*, 2017, **65**, 410–413.

36 X. Li, Z. Yang and Y. Peng, *New J. Chem.*, 2018, **42**, 4940–4950.

37 G. Kaur, S. Bharti and S. K. Tripathi, *J. Lumin.*, 2018, **195**, 375–384.

38 L. Liu, X. Wang, S. Zhu, C. Yao, D. Ban, R. Liu, L. Li and S. Wang, *Chem. Mater.*, 2019, **32**, 438–447.

39 L. Bazina, A. Maravić, L. Krce, B. Soldo, R. Odžak, V. B. Popović, I. Aviani, I. Primožič and M. Šprung, *Eur. J. Med. Chem.*, 2019, **163**, 626–635.

40 J. M. Stokes, C. R. MacNair, B. Ilyas, S. French, J.-P. Côté, C. Bouwman, M. A. Farha, A. O. Sieron, C. Whitfield and B. Coombes, *Nat. Microbiol.*, 2017, **2**, 1–8.

41 F. Rabanal and Y. Cajal, *Nat. Prod. Rep.*, 2017, **34**, 886–908.

42 C. R. Raetz and C. Whitfield, *Annu. Rev. Biochem.*, 2002, **71**, 635–700.

